Simulation of Dynamic Truck Loading on Pavements Using Measured Road Roughness

JUNGHSEN LIEH AND WEIGANG QI

Simulation results of truck dynamic loading based on measured road profiles are presented. Two truck configurations—two-axle straight trucks and five-axle tractor semitrailers—are used. The sprung mass (tractor and semitrailer) is modeled with bounce, roll, and pitch motions, and the unsprung mass (axle) has bounce and roll degrees of freedom. The suspension element is treated as a spring rate, a Coulomb friction, and a viscous damping coefficient. Tires are considered as linear springs with damping coefficients. Equations of motion were formulated from the separated-form virtual work principle, which automatically eliminates redundant coordinates. Computer programs developed on a personal computer include three portions: nonlinear integration, statistical analysis, and graphics. Runge-Kutta-Fehlberg's fourth-fifth-order algorithm with self-adjustable step sizes was adopted to solve the nonlinear truck equations. Numerical and graphical outputs can be provided in both time domain and statistical forms. Pavement profiles of both paths were measured by noncontact profilometers of the Ohio Department of Transportation and used as inputs to the program. Three levels of road roughness for each of concrete and asphalt pavements, as well as three vehicle forward speeds, were used in the simulation. The results show that the dynamic force can deviate significantly from the static loading. A statistical analysis indicates that the axle loading may be described by a Gaussian (normal) distribution. The standard deviation (or dynamic load coefficient) is affected by the vehicle forward speed and the pavement roughness.

Interest in understanding the manner in which heavy vehicles damage highway pavements has increased recently. It is well known that many factors affect the pavement performance; typical examples are pavement materials, temperature, traffic volume, road roughness, truck configuration, suspension type, and tire properties. The current approach for pavement analysis and design, taxation, fund allocation, and pavement management is based on static weights of various truck configurations. Traffic information used in design equations of AASHTO's *Guide for Design of Pavement Structures* (*1*) includes static axle loading, truck configurations, and frequency of load applications. The number of axle load applications is the cumulative 80 000-N (18,000-lb) equivalent single-axle loads (ESALs). The mixed traffic flow of different vehicles is converted into the ESAL number using estimated load equivalency factors or axle damage factors without considering the effect of road roughness and vehicle dynamics. The theoretical load equivalency factors were established using the exponential ratio of the calculated pavement response to that of the standard axle (*2*). The mechanistic method adopts measured strains or deflections from actual roadways rather than theoretical values (*3*). The load equivalency factor varies with the structural number and terminal serviceability index.

Static ESAL methods for pavement analysis and design may not be accurate because they neglect the dynamic effect of road excitations, suspensions, tires, inertia properties, and vehicle speeds. The actual pavement loading fluctuates above and below the static axle force. Current pavement analysis and design practices could oversimplify the interactive behavior between truck and pavement. From the dynamics point of view, these static approaches may underestimate the actual pavement loading (*4–7*).

Suspensions and tires have two major functions: to isolate sprung masses and freight from road excitations, and to provide guidance during braking, accelerating, and maneuvering (*8–13*). When a vehicle is under static equilibrium, each tire is subject to a static force distributed from the vehicle weight and geometry. As the vehicle is driven along the roadway, it experiences vibration due to the disturbance from the road surface. The disturbance deforms tires, develops tire forces, and then transmits these forces to axles, suspension elements, and sprung masses. The dynamic forces induced by the vibration of masses, springs, and tires are interactive and yield fluctuation in the pavement loading. The road roughness excites these forces and deteriorates the pavement. The deterioration will in turn yield higher loading on the roadway, thus speed up the process of pavement damage. After a very large number of alternating force cycles, fatigue failure could occur. It is obvious that the use of static ESALs for pavement analysis and design may not be adequate.

The axle loading could be measured with weigh-in-motion (WIM) installations. However, WIM instruments provide a very limited dynamic force spectrum because of cost and hardware constraints. Road simulators may also be used to determine the axle loading (*14*). Computer simulations have been used to study truck directional stability, braking and accelerating capability, rollover, and ride quality for many years. Such simulations have become increasingly sophisticated, starting with rudimentary models and advancing to recent multibody formulations (*15,16*).

The articulated vehicle models developed by Eschelman et al. (*17*) were used to examine handling capability without considering the roll degree of freedom. Detailed descriptions of truck simulation software—namely, linear yaw plane model, static roll model, yaw/roll model, and Phase IV program—were presented by Wong and El-Gindy (*18*) and Fancher and Mathew (*19*). The yaw plane model was derived to investigate the truck directional response (yaw and lateral) in a horizontal plane. The static roll program can only compute the rollover threshold of steady turning maneuvers

Mechanical and Materials Engineering, Wright State University, Dayton, Ohio 45435.

(i.e., the dynamic effect on rollover has been neglected). The yaw/roll model (*20–22*) was developed for evaluating the directional and roll responses of single- and multiple-trailer vehicles. The Phase IV program combined all existing computer codes into one program for simulating the truck braking and steering dynamics (*23*). Tabarrok and Tong (*24*) adopted a planar (horizontal) double doglogger model to examine the directional stability without incorporating the effect of suspension and tire stiffnesses. These programs can simulate only the vehicles moving over the horizontal road surface.

A half-tractor semitrailer model was used by El-Madany and El-Razaz (*25*) to design active suspensions. Ohta et al. (*26*) conducted a simulation and test on the ride quality using a two-dimensional straight truck model. Cebon (*7*), Hedrick et al. (*27*), and Karamihas and Gillespie (*28*) used pitch-plane truck models to predict the pavement loading. Hedrick and Yi (*29*) utilized planar truck models to evaluate the effect of semiactive suspensions on the flexible pavement response. A two-dimensional model provides the vehicle response in the vertical-longitudinal plane by neglecting the roll degrees of freedom of sprung and unsprung masses. To precisely predict the pavement loading, it will be necessary to superimpose three-dimensional truck dynamic models—that is, each sprung mass will contain bounce, roll, and pitch motions and each unsprung mass will have bounce and roll degrees of freedom. To mimic the real condition, measured road profiles are needed as the excitation input to the vehicle model.

The objective of this paper is to evaluate the dynamic pavement loading of heavy vehicles. The research work includes derivation of three-dimensional dynamic equations for two-axle straight trucks and five-axle tractor semitrailers as well as development of personal computer (PC) programs to estimate axle forces, thus providing engineers with better understanding of actual pavement loading. Computer simulations were based on the pavement roughness data measured with profilometers from the Ohio Department of Transportation (Ohio DOT). Nonlinear differential equations were solved using Runge-Kutta-Fehlberg's algorithm (RKF45). Tire forces and axle loadings were then computed. Three road profiles (low, medium, and high roughnesses) from each of asphalt and concrete pavements were collected from several roadways in Ohio. Results yielded from the simulation, originally in time domain, were converted into statistical forms. A procedure for graphics is also included in the program.

FORMULATION OF TRUCK DYNAMICS

The configuration of commercial vehicles ranges from straight trucks to tractor multiple-trailers. The tractor and trailers (full and semi) are connected through articulations (such as fifth wheel) that yield constraints and reduce the number of independent coordinates (or degrees of freedom). Equations of motion of a constrained system can be formulated using three approaches:

1. Treat redundant coordinates as part of unknowns and generate a large set of differential-algebraic equations with Lagrange multipliers.
2. Use a penalty formulation with a fictitious energy function,
3. Eliminate the redundant variables during formulation to generate a minimum set of differential equations.

To effectively formulate and solve equations of motion for commercial vehicles, the third method is adopted in this paper. The method is derived from the virtual work principle and may be described here:

$$\delta \underline{q}^T \sum_{i=1}^{n_r} [\underline{J}_{vi}^T (m_i \underline{a}_i - \underline{F}_i) + \underline{J}_{\omega i}^T (\dot{\underline{H}}_i - \underline{T}_i) - \underline{F}_{qi}] = 0 \tag{1}$$

where

$\underline{q}, \underline{F}_{qi} \in R^N$;
$\underline{a}_i, \underline{F}_i, \underline{H}_i, \underline{T}_i \in R^3$;
$\underline{J}_{vi}, \underline{J}_{\omega i} \in R^{3\times N}$.

The variable n_r is the number of rigid bodies, and N is the number of coordinates. For a constrained system, the coordinate vector q will contain dependent coordinates, therefore, the coefficient vector of $\delta \underline{q}$ will not vanish. It is necessary to divide $\underline{q}$ into an independent subvector and a redundant subvector.

Assume the constraint equations are expressed in the following kinematic form:

$$\underline{\phi}(\underline{q}, t) = \underline{0} \tag{2}$$

where $\underline{\phi}$ contains n independent equations (i.e., $\underline{\phi} \in R^n$). The vector $\underline{q}$ is partitioned into a redundant subvector $\underline{q}_r \in R^n$ and an independent subvector $\underline{x} \in R^{N-n}$, or $\underline{q} = [\underline{x}^T, \underline{q}_r^T]^T$. Differentiating and rearranging Equation 2 yields

$$\dot{\underline{q}} = \underline{\phi}_q \dot{\underline{x}} + \underline{D}_q \tag{3}$$

$$\delta \underline{q} = \underline{\phi}_q \delta \underline{x} \tag{4}$$

where $\underline{\phi}_q \in R^{N\times(N-n)}$ and $\underline{D}_q \in R^N$ with

$$\underline{\phi}_q = \begin{bmatrix} \underline{I} \\ -\left(\dfrac{\partial \underline{\phi}}{\partial \underline{q}_r}\right)^{-1} \dfrac{\partial \underline{\phi}}{\partial \underline{x}} \end{bmatrix} \tag{5a}$$

$$\underline{D}_q = \begin{bmatrix} \underline{0} \\ -\left(\dfrac{\partial \underline{\phi}}{\partial \underline{q}_r}\right)^{-1} \dfrac{\partial \underline{\phi}}{\partial t} \end{bmatrix} \tag{5b}$$

Equation 1 is further expanded in the following form using a Jacobian matrix expansion (*30*):

$$\underline{M}(\underline{q}, t)\ddot{\underline{x}} = \underline{f}_1(\dot{\underline{x}}, \underline{q}, t)\dot{\underline{x}} + \underline{f}_2(\underline{q}, t)\dot{\underline{x}} + \underline{f}_3(\underline{q}, t) + \underline{F}_e \tag{6}$$

In this equation,

$$\underline{M}(\underline{q}, t) = \sum_{i=1}^{n_r} \left\{ m_i \underline{J}_{vci}^T \underline{J}_{vci} + \underline{J}_{\omega ci}^T \underline{I}_i \underline{J}_{\omega ci} \right\} \tag{7a}$$

$$\underline{f}_1(\underline{\dot{x}},\underline{q},t)\underline{\dot{x}} = -\sum_{i=1}^{n_r}\left\{m_i \underline{J}_{vci}^T\left(\left[\frac{\partial J_{vcijk}}{\partial \underline{q}}\underline{\phi}_q \underline{\dot{x}}\right] + [\tilde{\underline{J}}_{\omega ci}\underline{\dot{x}}]\underline{J}_{vci}\right) + \underline{J}_{\omega ci}^T\left(\underline{I}_i\left[\frac{\partial J_{\omega cijk}}{\partial \underline{q}}\underline{\phi}_q \underline{\dot{x}}\right] + \left[\tilde{\underline{J}}_{\omega ci}\underline{\dot{x}}\right]\underline{I}_i\underline{J}_{\omega ci}\right)\right\}\underline{\dot{x}} \quad (7b)$$

$$\underline{f}_2(\underline{q},t)\underline{\dot{x}} = -\sum_{i=1}^{n_r}\left\{m_i\underline{J}_{vci}^T\left(\left[\frac{\partial J_{vcijk}}{\partial \underline{q}}\underline{\phi}_t + \frac{\partial J_{vcijk}}{\partial t}\right]\underline{\dot{x}} + [\tilde{\underline{J}}_{\omega ci}\underline{\dot{x}}]\underline{V}_{ti} + \tilde{\underline{\omega}}_{ti}\underline{J}_{vci}\underline{\dot{x}} + \frac{\partial \underline{V}_{ti}}{\partial \underline{q}}\underline{\phi}_q\underline{\dot{x}}\right) + \underline{J}_{\omega ci}^T\left(\underline{I}_i\left[\frac{\partial J_{\omega cijk}}{\partial \underline{q}}\underline{\phi}_t + \frac{\partial J_{\omega cijk}}{\partial t}\right]\underline{\dot{x}} + [\tilde{\underline{J}}_{\omega ci}\underline{\dot{x}}]\underline{I}_i\underline{\omega}_{ti} + \tilde{\underline{\omega}}_{ti}\underline{I}_i\underline{J}_{\omega ci}\underline{\dot{x}} + \underline{I}_i\frac{\partial \underline{\omega}_{ti}}{\partial \underline{q}}\underline{\phi}_q\underline{\dot{x}}\right)\right\} \quad (7c)$$

$$\underline{f}_3(\underline{q},t) = -\sum_{i=1}^{n_r}\left\{m_i\underline{J}_{vci}^T\left(\tilde{\underline{\omega}}_{ti}\underline{V}_{ti} + \frac{\partial \underline{V}_{ti}}{\partial \underline{q}}\underline{\phi}_t + \frac{\partial \underline{V}_{ti}}{\partial t}\right) + \underline{J}_{\omega ci}^T\left(\tilde{\underline{\omega}}_{ti}\underline{I}_i\underline{\omega}_{ti} + \underline{I}_i\frac{\partial \underline{\omega}_{ti}}{\partial \underline{q}}\underline{\phi}_t + \underline{I}_i\frac{\partial \underline{\omega}_{ti}}{\partial t}\right)\right\} \quad (7d)$$

$$\underline{F}_e = \sum_{i=1}^{n_r}\left\{\underline{J}_{vci}^T\underline{F}_i + \underline{J}_{\omega ci}^T\underline{T}_i + \underline{F}_{xi}\right\} \quad (7e)$$

On the basis of this formulation procedure, equations of motion of two truck configurations were generated. The straight truck model consists of a sprung mass and two unsprung masses (axles), and the tractor semitrailer contains two articulated sprung masses and five unsprung masses, as shown in Figure 1. The suspension element is represented by a spring rate, a Coulomb friction, and a viscous damping coefficient. Tires are treated as linear springs with viscous damping. With small motion, the equations of motion may be linearized and rearranged into a second-order form:

$$\underline{M}\,\ddot{\underline{x}} + \underline{C}\,\dot{\underline{x}} + \underline{K}\,\underline{x} = \underline{B}_1\underline{w} + \underline{B}_2\,\dot{\underline{w}} + \underline{B}_3\,\underline{F} \quad (8)$$

where

$\underline{M}$, $\underline{C}$, $\underline{K}$ = mass, damping, and stiffness matrices, respectively;
$\underline{w}$ = disturbance vector; and
$\underline{F}$ = friction force vector.

To facilitate numerical integration, Equation 8 is further converted into a state-space form

$$\dot{\underline{y}} = \underline{A}\,\underline{y} + \underline{B}_1^*\,\underline{w} + \underline{B}_2^*\,\dot{\underline{w}} + \underline{B}_3^*\underline{F} \quad (9)$$

where the state vector

$$\underline{y} = [\underline{x}^T, \dot{\underline{x}}^T]^T \quad (10)$$

For the two-axle straight truck, the number of degrees of freedom is seven (DOF = 7). The state $\underline{y}$ as described in Equation 9 is a 14×1 vector. For the five-axle tractor semitrailer model, 16 coordinates and a constraint are defined. The constraint is induced by the articulation and is used to substitute the bounce (q_{16}) of the semitrailer with the bounce (q_1) and pitch (q_3) of the tractor as well as the pitch (q_{11}) of the semitrailer. The number of degrees of freedom is therefore reduced to 15 (DOF = 15), and the state y becomes a 30×1 vector.

The profile vector w contains time delays in the second and following axles and may be written as

$$\underline{w} = [w_1(t), w_2(t), w_1(t-\tau_2), w_2(t-\tau_2), \ldots, w_1(t-\tau_\kappa), w_2(t-\tau_\kappa)]^T \quad (11)$$

where w_1 and w_2 are the road profiles of left and right paths, respectively, and k is 2 for two-axle vehicles and 5 for five-axle vehicles. The time delay depends on the axle distance (L_i) as well as the vehicle forward speed (v), and is defined by

$$\tau_i = \frac{L_i}{v} \quad (12)$$

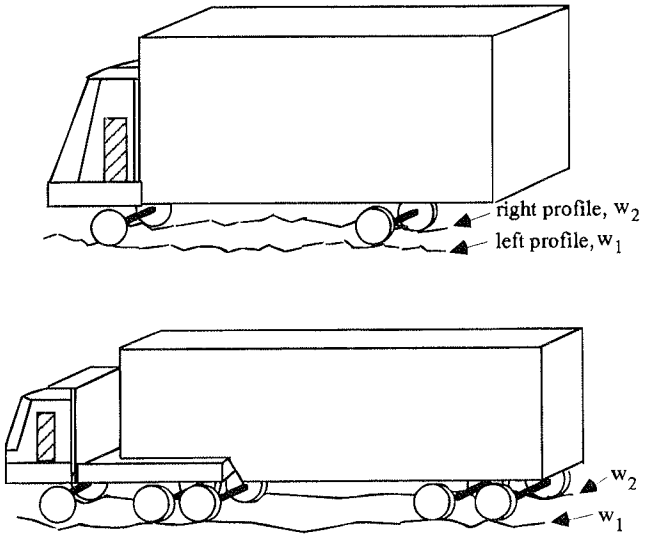

FIGURE 1 Configurations of straight truck (*top*) and tractor semitrailer (*bottom*) used in study.

NUMERICAL SOLUTION

Several numerical integration schemes such as Runge-Kutta methods and predictor-corrector methods may be used to solve ordinary differential equations. The selection of the integration algorithm is based on accuracy, efficiency, and numerical stability. In the present study, a Fehlberg's fourth-fifth-order algorithm of Runge-Kutta method (RKF45) is adopted because of its capability to self-adjust the step size by the local truncation error and a convergence factor. Define the righthand side of Equation 9 as

$$\underline{f}(\underline{y}, t) = \underline{A}\,\underline{y} + \underline{B}_1^*\,\underline{w} + \underline{B}_2^*\,\dot{\underline{w}} + \underline{B}_3^*\,\underline{F} \quad (13)$$

The equations for the RKF45 method are given here (*31*):

$$ {}^4\underline{y}_{i+1} = {}^4\underline{y}_i + \left(\frac{25}{216}\underline{k}_1 + \frac{1,408}{2,565}\underline{k}_3 + \frac{2,197}{4,104}\underline{k}_4 - \frac{1}{5}\underline{k}_5 \right) h \tag{14} $$

$$ {}^5\underline{y}_{i+1} = {}^5\underline{y}_i + \left(\frac{16}{135}\underline{k}_1 + \frac{6,656}{12,825}\underline{k}_3 + \frac{28,561}{56,430}\underline{k}_4 - \frac{9}{50}\underline{k}_5 + \frac{2}{55}\underline{k}_6 \right) h \tag{15} $$

where

$$ \underline{k}_1 = 2\underline{f}(\underline{y}_i, t_i) $$

$$ \underline{k}_2 = \underline{f}\left(\underline{y}_i + \frac{1}{4}h\underline{k}_1, t_i + \frac{1}{4}h\right) $$

$$ \underline{k}_3 = \underline{f}\left(\underline{y}_i + \frac{3}{32}h\underline{k}_1 + \frac{9}{32}h\underline{k}_2, t_i + \frac{3}{8}h\right) $$

$$ \underline{k}_4 = \underline{f}\left(\underline{y}_i + \frac{1,932}{2,197}h\underline{k}_1 - \frac{7,200}{2,197}h\underline{k}_2 + \frac{7,296}{2,197}h\underline{k}_3, t_i + \frac{12}{13}h\right) $$

$$ \underline{k}_5 = \underline{f}\left(\underline{y}_i + \frac{439}{216}h\underline{k}_1 - 8h\underline{k}_2 + \frac{3,680}{513}h\underline{k}_3 - \frac{845}{4,104}h\underline{k}_4, t_i + h\right) $$

$$ \underline{k}_6 = \underline{f}\left(\underline{y}_i - \frac{8}{27}h\underline{k}_1 + 2h\underline{k}_2 - \frac{3,544}{2,565}h\underline{k}_3 + \frac{1,859}{4,104}h\underline{k}_4 + \frac{11}{40}h\underline{k}_5, t_i + \frac{1}{2}h\right) $$

The local truncation error is estimated as the difference between Equations 14 and 15, that is,

$$ \Delta\underline{y}_{i+1} = {}^5\underline{y}_{i+1} - {}^4\underline{y}_{i+1} = \left(\frac{1}{360}\underline{k}_1 - \frac{128}{4,275}\underline{k}_3 - \frac{2,197}{75,240}\underline{k}_4 + \frac{1}{50}\underline{k}_5 + \frac{2}{55}\underline{k}_6 \right) h \tag{16} $$

The solution determined from RKF45 consists of the vibration information of a vehicle, that is, displacements (q_i) and velocities ($\dot{q}_i$) of bounce, pitch, and roll. These data are not stored on the disk because they require so much memory (however, they can be written out to the disk if necessary). These displacements and velocities are used to calculate tire contact forces and axle loadings. Tire forces are computed using the tire stiffness, bounce, and roll motions of each axle, as well as road profiles, and may be expressed as follows:

Tire force of the steering axle:

$$ {}^1F_{t1,2} = K_{t1}\left[w_{1,2} - \left(q_4 \pm \frac{y_{t1}}{2} q_5 \right) \right] + C_{t1}\left[\dot{w}_{1,2} - \left(\dot{q}_4 \pm \frac{y_{t1}}{2}\dot{q}_5 \right) \right] + \frac{f_{as1}}{2} \tag{17} $$

Tire forces of the second and following axles (dual tire space s_i = 0 for inner tires):

$$ {}^iF_{t1-4} = K_{ti}\left[w_{1,2}(t-\tau_i) - \left(q_j \pm \left(\frac{y_{ti}}{2} + s_i \right) q_{j+1} \right) \right] + C_{ti}\left[\dot{w}_{1,2}(t-\tau_i) - \left(\dot{q}_j \pm \left(\frac{y_{ti}}{2} + s_i \right)\dot{q}_{j+1} \right) \right] + \frac{f_{asi}}{4} \tag{18} $$

where K_{ti}, C_{ti}, and F_{asi} are the tire stiffness, tire damping, and static loading of each axle. It can be seen that both axle bounce and roll appear in tire force equations. Since the truck equations are coupled, the axle bounce and roll are interactive with other degrees of freedom. The tire stiffness, tire damping, and road roughness obviously will affect dynamic tire forces. The suspensions as well as the truck inertia and geometry characteristics will also influence the tire force through the coupled truck equations.

The dynamic axle loading is computed by adding the corresponding tire contact forces, that is,

$$ F_{ai} = \sum_k {}^iF_{tk} \tag{19} $$

STATISTICAL ANALYSIS

The numerical values obtained from RKF45 are in time domain. For statistical analysis, each time history can be converted into a mean, a standard deviation, a density function, and a probability distribution. The mean value is expressed as follows:

$$ \mu = \frac{1}{N}\sum_{i=1}^{N} x_i \tag{20} $$

where N is the number of data points and x_i represents the force variable. The standard deviation is determined using

$$ \sigma = \sqrt{\frac{1}{N}\sum_{i=1}^{N}(x_i - \mu)^2} \tag{21} $$

The discrete probability density is approximated by

$$ f_d(x) \cong \frac{1}{\Delta x}\frac{N_{\Delta x}}{N} \tag{22} $$

where Δx is the interval of the loading (equal spacing is used) and $N_{\Delta x}$ is the number of points extracted from the corresponding force interval. The discrete probability density is compared with the density of a normal distribution:

$$ f(x) = \frac{1}{\sqrt{2\pi}\sigma} e^{-(x-\mu)^2/2\sigma^2} \tag{23} $$

The dynamic load coefficient (DLC) is defined as the ratio of the standard deviation to the static force:

$$ \text{DLC} = \frac{\text{standard deviation of axle loading}}{\text{static (or mean) axle loading}} = \frac{\sigma}{\mu} \tag{24} $$

RESULTS

The PC programs developed from the preceding procedures use the measured road roughness as the input excitation. The profile data were collected with Ohio DOT's profilometer model 690DNC. The original data were stored in a binary format with a DEC PDP computer and converted into the ASCII code. Each roughness file con-

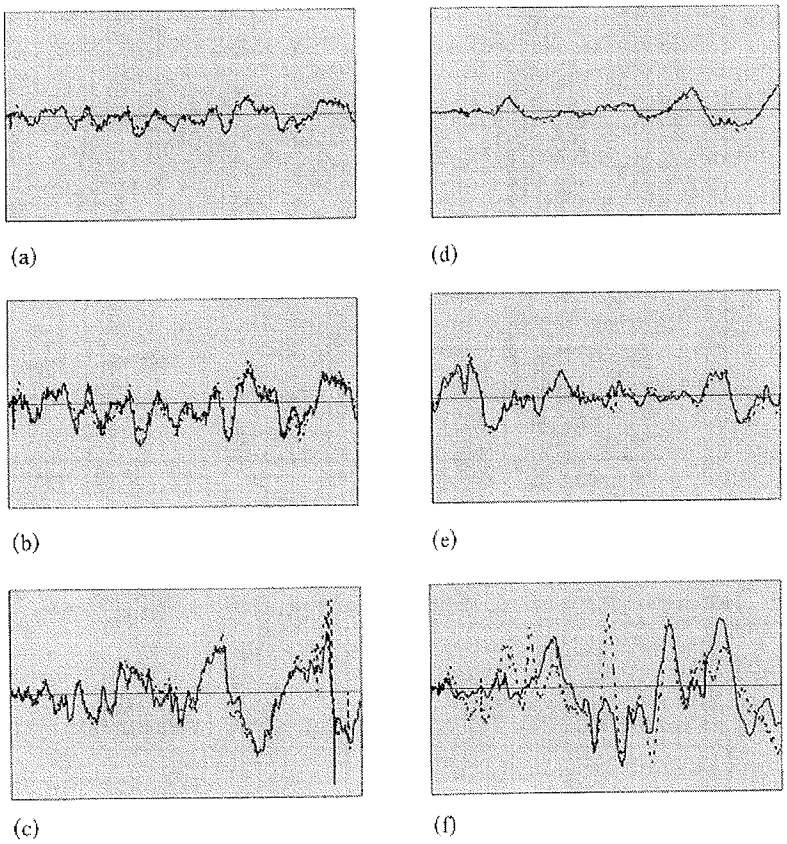

FIGURE 2 Road roughness used in study (partially shown only): *a*, low-roughness concrete pavement; *b*, medium-roughness concrete pavement; *c*, high-roughness concrete pavement; *d*, low-roughness asphalt pavement; *e*, medium-roughness asphalt pavement; *f*, high-roughness asphalt pavement.

tains three columns of data: the vehicle travel distance and a pair of vertical displacements of road surface (one for each wheel path). The roughness data points were taken every 2 in., averaged over a 12-in. period, and stored on the disk for every 6 in. of travel.

Results based on three levels of road surface (low, medium, and high roughness) of each of concrete and asphalt pavements are presented. The road profiles are partially shown in Figure 2. These six roughness data files include the following:

- CONLO: a concrete pavement of low roughness with a Mays ride number of 61.2,
- CONMD: a concrete pavement of medium roughness with a Mays ride number of 116.7,
- CONHI: a concrete pavement of high roughness with a Mays ride number of 219.7,
- ASPLO: an asphalt pavement of low roughness with a Mays ride number of 44.9,
- ASPMD: an asphalt pavement of medium roughness with a Mays ride number of 91, and
- ASPHI: an asphalt pavement of high roughness with a Mays ride number of 145.

The simulation program first computes the state variables (i.e., displacements and velocities of bounce, roll, and pitch). It then calculates tire forces and axle loadings and converts the time domain solution into statistical forms (i.e., mean, standard deviation, probability density, and distribution). Three vehicle speeds: 48, 80, and 113 km/hr (30, 50, and 70 mph) were used in the study.

Figure 3 shows the time history of the second axle loading of the straight truck on high-roughness concrete pavement. It can be seen that the axle loading is severely excited at certain locations. Figure 4 illustrates the probability density of the same axle on medium-roughness asphalt pavement. The probability density is similar to a normal distribution. The standard deviation, DLC, and maximum value of the second axle loading are given in Tables 1 and 2. This table indicates that the DLC and the maximum axle loading are affected significantly by the roughness and vehicle speed.

Similar results are observed for the five-axle tractor semitrailer model (Figures 5 through 7). The standard deviations, DLCs, and maximum values of axle loading are presented in Tables 3 through 8. As is expected, the dynamic axle loading is influenced by the pavement roughness and vehicle speed. For the pavement profiles used in the study, the severest axle loading could reach more than twice the static loading, and the greatest DLC is more than 20 percent.

SUMMARY

Equations of motion for two truck configurations were derived using the virtual work principle. The vehicle models contain bounce, roll, and pitch degrees of freedom for each sprung mass

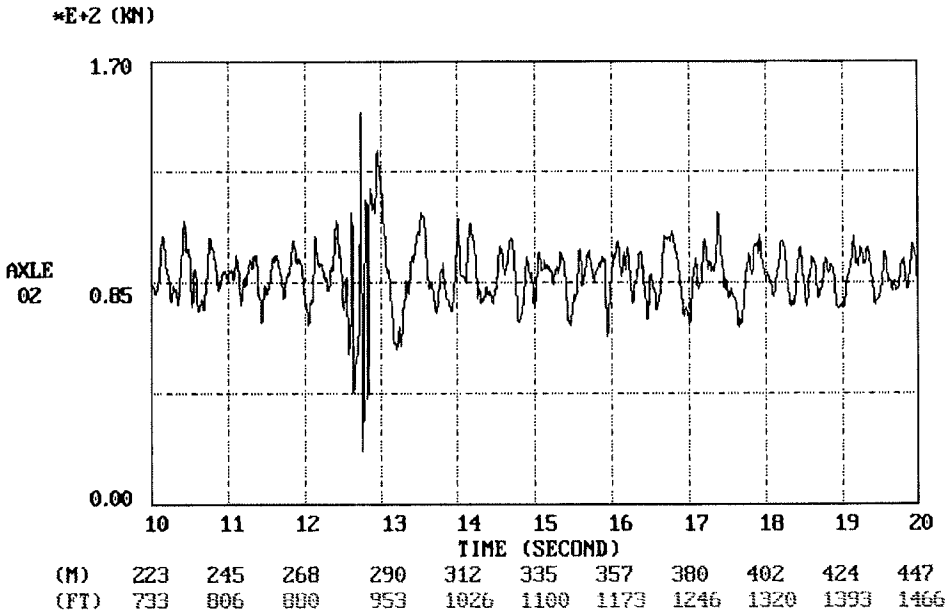

FIGURE 3 Two-axle truck second axle loading on high-roughness concrete pavement, $v = 80$ km/hr (50 mph).

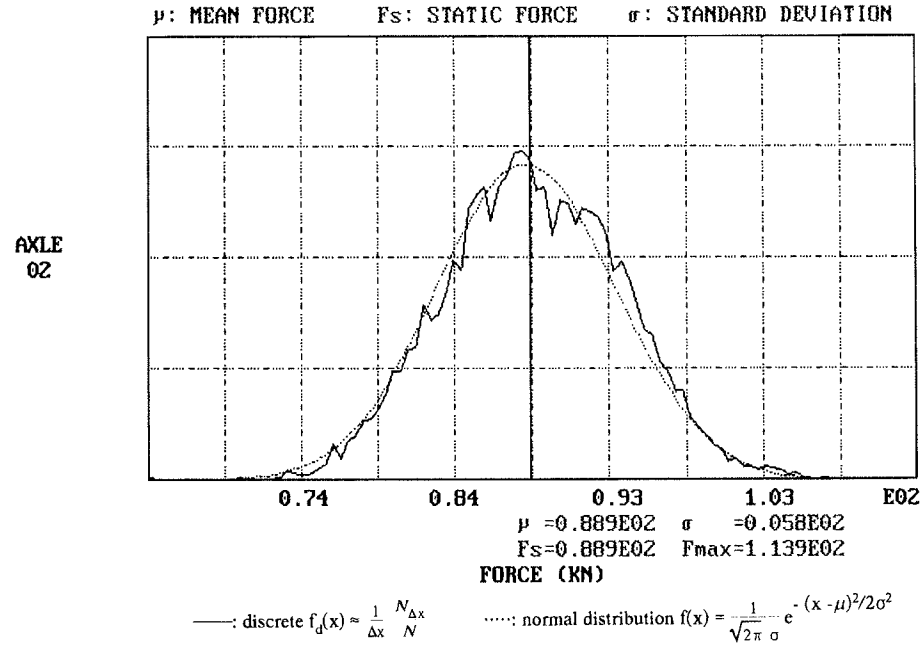

FIGURE 4 Two-axle truck probability density of second axle loading on medium-roughness asphalt pavement, $v = 80$ km/hr (50 mph).

TABLE 1 Two-Axle Truck Second Axle Loading: Standard Deviation σ, Normalized Values σ/F_s and $(F_{max} - F_s)/F_s$ ($F_s = 89$ kN)

Stand. Dev. (DLC*)	km/hr	CONLO	CONMD	CONHI	ASPLO	ASPMD	ASPHI
σ ($\frac{\sigma}{F_s}$)	48	4.744 (5.33%)	6.116 (6.88%)	7.442 (8.37%)	4.478 (5.03%)	5.269 (5.92%)	5.329 (5.99%)
	80	4.608 (5.18%)	6.187 (6.95%)	9.778 (10.99%)	3.894 (4.38%)	5.897 (6.63%)	5.593 (6.29%)
	113	6.036 (6.79%)	7.298 (8.20%)	12.365 (13.90%)	4.931 (5.54%)	7.960 (8.95%)	8.729 (9.81%)

* DLC = Dynamic Load Coefficient

TABLE 2 Two-Axle Truck Second Axle Loading: Maximum Axle Loading F_{max}, Normalized Values σ/F_s and $(F_{max} - F_s)/F_s$ ($F_s = 89$ kN)

Maximum Axle Force	km/hr	CONLO	CONMD	CONHI	ASPLO	ASPMD	ASPHI
F_{max} ($\frac{F_{max} - F_s}{F_s}$)	48	103.19 (+16.0%)	105.73 (+18.9%)	157.94 (+77.5%)	105.05 (+18.1%)	107.57 (+20.9%)	111.42 (+25.2%)
	80	109.48 (+23.1%)	111.32 (+25.1%)	151.74 (+70.6%)	105.84 (+19.0%)	113.93 (+28.1%)	113.34 (+27.4%)
	113	114.52 (+28.7%)	114.75 (+29.0%)	149.01 (+67.5%)	109.03 (+22.6%)	117.02 (+31.5%)	120.09 (+35.0%)

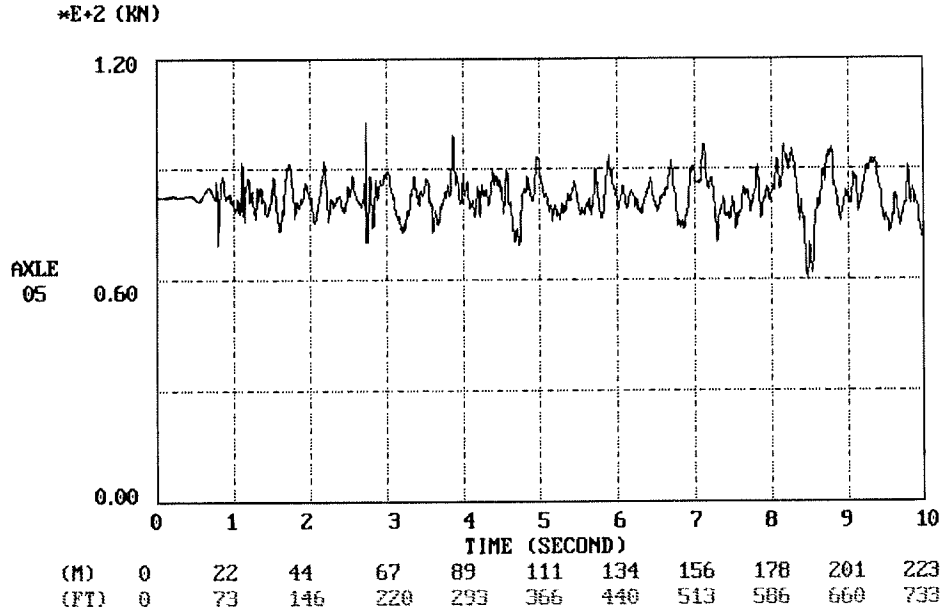

FIGURE 5 Five-axle tractor semitrailer fifth axle loading on high-roughness asphalt pavement, v = 80 km/hr (50 mph).

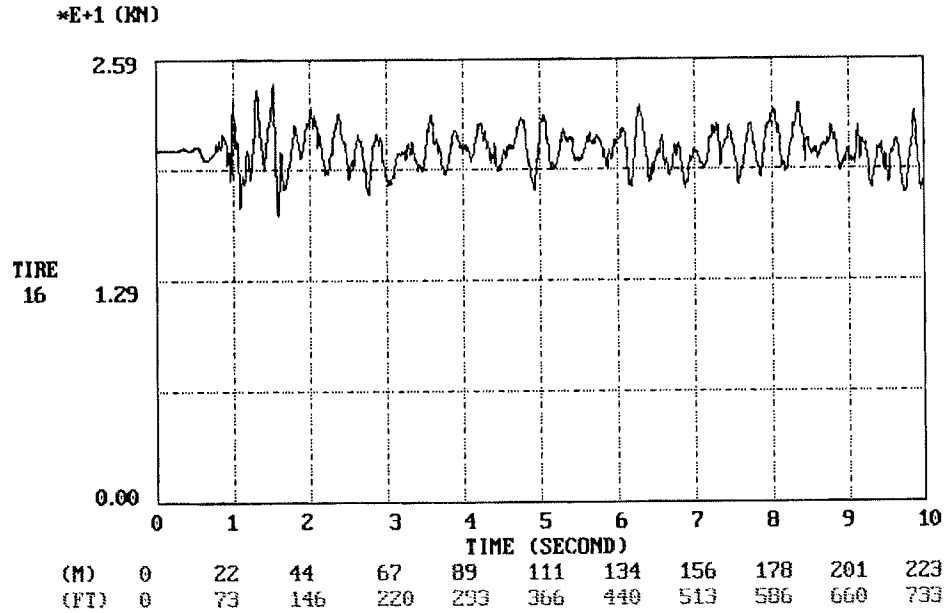

FIGURE 6 Five-axle tractor semitrailer 16th tire contact force on low-roughness concrete pavement, v = 80 km/hr (50 mph).

(tractor and semitrailer), and each unsprung mass (axle) consists of bounce and roll degrees of freedom. Each suspension element is represented by a spring rate, a Coulomb friction, and a damping coefficient. Tires are treated as linear springs and viscous dampers. Fehlberg's version of Runge-Kutta fourth-fifth-order integration algorithm with self-adjustable step sizes was adopted to solve the nonlinear truck equations. Using these equations, computer programs were developed. Pavement profiles measured by Ohio DOT's profilometers were used as the input excitation to the vehicle models. In addition to simulation programs, a subroutine for graphical outputs is also provided. The software was developed in a user-friendly environment, allowing users to run programs easily.

Three pavement profiles (low, medium, and high roughness) for each of concrete and asphalt pavements, and three vehicle speeds [48, 80, and 113 km/hr (30, 50, and 70 mph)] were included in the simulation. Tire contact forces and axle loadings obtained from simulations can be presented in both time domain and statistical forms. The results show that the dynamic loading may deviate significantly from the static loading. For the pavement roughnesses used in the study, the maximum axle loading was observed to be

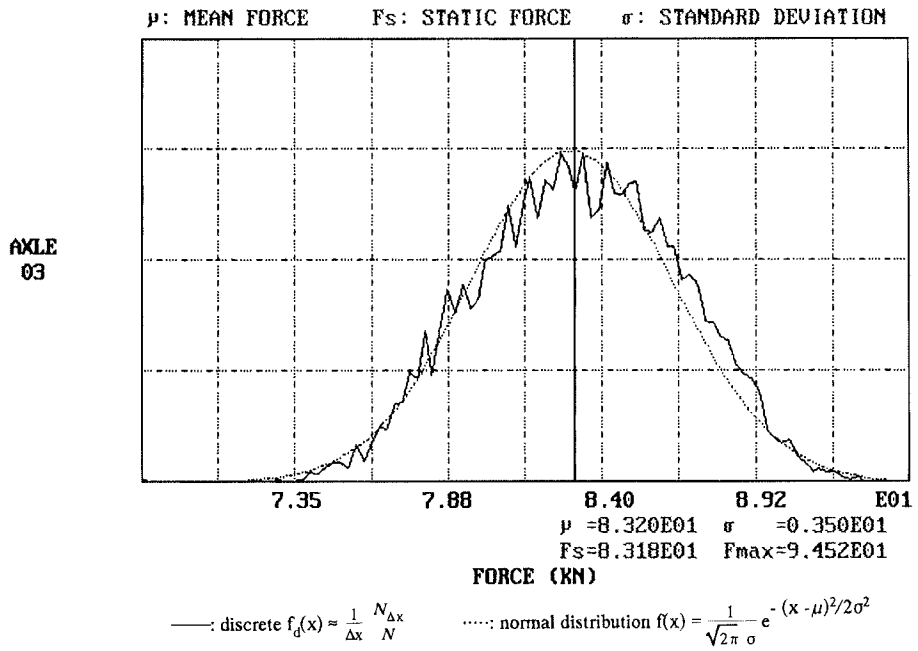

FIGURE 7 Five-axle tractor semitrailer probability density of third axle loading on medium-roughness concrete pavement, v = 48 km/hr (30 mph).

TABLE 3 Five-Axle Tractor Semitrailer First Axle Loading: Standard Deviation σ, Normalized Values σ/F_s and $(F_{max} - F_s)/F_s$ (F_s = 53.9 kN)

Stand. Dev. (DLC*)	km/hr	CONLO	CONMD	CONHI	ASPLO	ASPMD	ASPHI
σ ($\frac{\sigma}{F_s}$)	48	2.344 (4.35%)	2.929 (5.43%)	3.888 (7.21%)	2.431 (4.51%)	2.423 (4.49%)	2.527 (4.69%)
	80	2.936 (5.44%)	3.395 (6.29%)	4.887 (9.06%)	2.689 (4.99%)	3.297 (6.11%)	3.116 (5.78%)
	113	2.782 (5.16%)	3.882 (7.20%)	6.323 (11.72%)	2.782 (5.16%)	4.077 (7.56%)	4.592 (8.51%)

* DLC = Dynamic Load Coefficient

TABLE 4 Five-Axle Tractor Semitrailer First Axle Loading: Maximum Axle Loading F_{max}, Normalized Values σ/F_s and $(F_{max} - F_s)/F_s$ (F_s = 53.9 kN)

Maximum Axle Force	km/hr	CONLO	CONMD	CONHI	ASPLO	ASPMD	ASPHI
F_{max} ($\frac{F_{max} - F_s}{F_s}$)	48	61.305 (+13.7%)	62.422 (+15.7%)	88.819 (+64.7%)	61.432 (+13.9%)	62.431 (+15.8%)	66.695 (+23.7%)
	80	64.596 (+19.8%)	64.886 (+20.3%)	88.204 (+63.5%)	64.225 (+19.1%)	67.086 (+24.4%)	67.970 (+26.0%)
	113	63.564 (+17.9%)	65.319 (+21.1%)	89.321 (+65.6%)	63.564 (+17.9%)	68.518 (+27.0%)	74.035 (+37.3%)

TABLE 5 Five-Axle Tractor Semitrailer Second Axle Loading: Standard Deviation σ, Normalized Values σ/F_s and $(F_{max} - F_s)/F_s$ (F_s = 83.2 kN)

Stand. Dev. (DLC*)	km/hr	CONLO	CONMD	CONHI	ASPLO	ASPMD	ASPHI
σ ($\frac{\sigma}{F_s}$)	48	2.656 (3.19%)	3.657 (4.40%)	10.724 (12.89%)	2.864 (3.44%)	3.527 (4.24%)	3.441 (4.14%)
	80	2.897 (3.48%)	4.193 (5.04%)	9.592 (11.53%)	2.946 (3.54%)	4.238 (5.09%)	4.477 (5.38%)
	113	3.642 (4.38%)	5.999 (7.21%)	15.506 (18.64%)	3.642 (4.38%)	6.899 (8.29%)	8.489 (10.20%)

* DLC = Dynamic Load Coefficient

TABLE 6 Five-Axle Tractor Semitrailer Second Axle Loading: Maximum Axle Loading F_{max}, Normalized Values σ/F_s and $(F_{max} - F_s)/F_s$ (F_s = 83.2 kN)

Maximum Axle Force	km/hr	CONLO	CONMD	CONHI	ASPLO	ASPMD	ASPHI
F_{max} ($\frac{F_{max} - F_s}{F_s}$)	48	96.006 (+15.4%)	96.217 (+15.7%)	216.18 (+159.9%)	93.310 (+12.2%)	100.67 (+21.0%)	103.31 (+24.2%)
	80	99.632 (+19.8%)	103.83 (+24.8%)	169.85 (+104.2%)	98.753 (+18.7%)	102.58 (+23.3%)	105.52 (26.9%)
	113	105.76 (+27.1%)	113.81 (+36.8%)	194.56 (+133.9%)	105.76 (+27.1%)	113.87 (+36.9%)	119.49 (+43.6%)

TABLE 7 Five-Axle Tractor Semitrailer Fifth Axle Loading: Standard Deviation σ, Normalized Values σ/F_s and $(F_{max} - F_s)/F_s$ (F_s = 83.4 kN)

Stand. Dev. (DLC*)	km/hr	CONLO	CONMD	CONHI	ASPLO	ASPMD	ASPHI
σ ($\frac{\sigma}{F_s}$)	48	3.290 (3.95%)	4.186 (5.02%)	5.702 (6.84%)	3.187 (3.82%)	3.848 (4.62%)	3.815 (4.58%)
	80	4.019 (4.82%)	5.112 (6.13%)	10.773 (12.92%)	4.376 (5.25%)	5.027 (6.03%)	5.080 (6.09%)
	113	4.806 (5.77%)	6.260 (7.51%)	11.358 (13.63%)	4.806 (5.77%)	6.651 (7.98%)	7.010 (8.41%)

* DLC = Dynamic Load Coefficient

TABLE 8 Five-Axle Tractor Semitrailer Fifth Axle Loading: Maximum Axle Loading F_{max}, Normalized Values σ/F_s and $(F_{max} - F_s)/F_s$ (F_s = 83.4 kN)

Maximum Axle Force	km/hr	CONLO	CONMD	CONHI	ASPLO	ASPMD	ASPHI
F_{max} ($\frac{F_{max} - F_s}{F_s}$)	48	95.332 (+14.4%)	95.674 (+14.8%)	146.67 (+76.0%)	95.782 (+14.9%)	94.811 (+13.7%)	101.43 (+21.7%)
	80	97.590 (+17.1%)	105.82 (+27.0%)	184.51 (+121.4%)	97.107 (+16.5%)	101.93 (+22.3%)	106.37 (+27.6%)
	113	102.24 (+22.7%)	107.44 (+28.9%)	175.04 (+110.0%)	102.24 (+22.7%)	110.20 (+32.2%)	109.29 (+31.1%)

more than twice the static loading. A statistical analysis indicates that the pavement loading may be described by a Gaussian (normal) distribution. The standard deviation, DLC, and maximum loading are affected by the pavement roughness and vehicle speed.

Computer simulation of common truck models traveling over real pavement profiles improves the understanding of tire and axle loadings. Procedures developed in this paper may be used to improve design procedures and design inputs associated with these structures and more accurately estimate remaining useful life. Computerized methods would reduce the evaluation cost and time. The dynamic axle loading may also be used in the future to control the legal load limit, taxation, penalties, and pavement design and analysis by federal and state departments of transportation.

ACKNOWLEDGMENTS

The research work was sponsored by Ohio DOT, FHWA, and Wright State University. The measured road profiles were provided by Ohio DOT. Inputs and valuable suggestions from Roger Green, Emil Marginean, Bill Edwards, James Sargeant, Ken Corns, and Bob Jessberger of Ohio DOT are highly appreciated.

REFERENCES

1. *Guide for Design of Pavement Structures.* AASHTO, Washington, D.C., 1993.
2. Treybig, H. J. *Equivalency Factor Development for Multiple Axle Configurations.* In *Transportation Research Record 949*, TRB, National Research Council, Washington, D.C., 1983, pp. 32–44.
3. Hutchinson, B. G., et al. Equivalencies of Different Axle Load Groups. *Proc., 2nd North American Conference on Managing Pavements*, Vol. 3, 1987, pp. 3.191–3.202.
4. Robinson, R. G. *Trends in Axle Loading and Their Effect on Design of Road Pavements.* Research Report 138. Transport and Road Research Laboratory, Crowthorne, Berkshire, England, 1988.
5. Cebon, D., and C. B. Winkler. *A Study of Road Damage Due to Dynamic Wheel Loads Using a Load Measuring Mat.* Report UMTRI-90-13, SHRP-87-ID015/MDOT-89-0583. University of Michigan Transportation Research Institute, Ann Arbor, 1990.
6. Mamlouk, M. S. Rational Look at Truck Axle Weight. In *Transportation Research Record 1307*, TRB, National Research Council, Washington, D.C., 1991.
7. Cebon, D. *Interaction Between Heavy Vehicles and Roads.* Report SP 951. SAE, Warrendale, Pa., 1993.
8. Bastow, D. *Car Suspensions and Handling.* Pentech, London, 1987.
9. Dixon, J. C. *Tires, Suspension and Handling.* Cambridge University Press, England, 1991.
10. Gillespie, T. D. *Fundamentals of Vehicle Dynamics.* SAE, Warrendale, Pa., 1992.
11. Lieh, J. The Effect of Bandwidth of Semiactive Dampers on Vehicle Ride. *Journal of Dynamic Systems, Control and Measurement*, Vol. 115, 1993, pp. 571–575.
12. Wong, J. Y. *Theory of Ground Vehicles*, 2nd ed. John Wiley & Sons, New York, 1993.
13. Fitch, J. W. *Motor Truck Engineering Handbook*, 4th ed. SAE, Warrendale, Pa., 1994.
14. Hu, G. Use of a Road Simulator for Measuring Dynamic Wheel Loads. In *SP 765: Vehicle/Pavement Interaction Where the Truck Meets the Road*, SAE, Warrendale, Pa., 1988, pp. 61–68.
15. Lieh, J., and I. Haque. Symbolic Closed-Form Modeling and Linearization of Multibody Systems Subject to Control. *Journal of Mechanical Design*, Vol. 113, 1991, pp. 124–132.
16. Lieh, J. An Alternative Method to Formulate Closed-Form Dynamics for Elastic Mechanical Systems Using Symbolic Process. *Mechanics of Structures and Machines*, Vol. 20, 1992, pp. 253–279.
17. Eschelman, R. L., et al. *Stability and Handling Criteria of Articulated Vehicles.* Final Report J6 281/DOT-HS 800915. Illinois Institute of Technology, Research Institute, Chicago, 1973.
18. Wong, J. Y., and M. El-Gindy. *Vehicle Weights and Dimensions Study, Computer Simulation of Heavy Vehicle Dynamic Behavior, Users Guide to the UMTRI Models.* Interim Technical Report. RTAC-ARTC, 1985.
19. Fancher, P. S., and A. Mathew. *A Vehicle Dynamics Handbook for Single-Unit and Articulated Heavy Trucks.* Final Report DOT-HS-807-185, UMTRI-86-37. 1987.
20. Mallikarjunarao, C., and L. Segel. A Study of The Directional and Roll Dynamics of Multiple-Articulated Vehicles: *Proc., 7th IASVD Symposium for Vehicle System Dynamics*, 1981, pp. 81–96.
21. Winkler, C. B., et al. *Improving the Dynamic Performance of Multitrailer Vehicles: A Study of Innovative Dollies—Volume I.* Report FHWA/RD-86-161, UMTRI-86-26/I. 1987.
22. El-Gindy, M., et al. Evaluation of the Dynamic Performance of Heavy Commercial Vehicles. *Proc., Advanced Automotive Technology, ASME Winter Annual Meeting*, Vol. 40, 1991, pp. 183–197.
23. MacAdam, C. C., et al. *A Computerized Model for Simulating the Braking and Steering Dynamics of Trucks, Tractor-Semitrailers, Doubles, and Triples Combinations—User's Manual—Phase 4.* Report, UM-HSREI-80-58. University of Michigan, Ann Arbor, 1980.
24. Tabarrok, B., and L. Tong. The Directional Stability Analysis of Log Hauling Truck—Double Doglogger. *Proc., Symposium on Transportation Systems, ASME Winter Annual Meeting*, Vol. 44, 1992, pp. 383–396.
25. El-Madany, M. M., and Z. S. El-Razaz. Performance of Actively Suspended Cabs in Highway Trucks—Evaluation and Optimization. *Journal of Sound and Vibration*, Vol. 126, 1988, pp. 423–435.
26. Ohta, M., et al. *The Influence of Tire Deformation on Ride Comfort of a Truck.* In SP 843, SAE, Warrendale, Pa., 1990, pp. 37–45.
27. Hedrick, J. K., M. J. Marlow, and B. Brademeyer. *The Simulation of Vehicle Dynamic Effects on Road Pavements.* Final Report FHWA-RD-90-108. FHWA, U.S. Department of Transportation 1992.
28. Karamihas, S. M., and T. D. Gillespie. Characterizing Trucks for Dynamic Load Prediction. *International Journal of Vehicle Design: Heavy Vehicle Systems*, Vol. 1, 1993, pp. 3–19.
29. Hedrick, J. K., and K. Yi. The Effect of Alternative Heavy Truck Suspensions on the Flexible Pavement Response. *Proc., 2nd International Symposium on Heavy Vehicle Weights and Dimensions*, Canada, 1987.
30. Lieh, J. Separated-Form Equations of Motion for Controlled Multibody Systems. *Journal of Dynamic Systems, Measurement and Control*, Vol. 116, Dec. 1994, pp. 702–712.
31. Chapra, S. C., and R. P. Canale. *Numerical Methods for Engineers*, 2nd ed. McGraw Hill, 1990.

Publication of this paper sponsored by Committee on Surface Properties–Vehicle Interaction.